3-2020

A theoretical first principles computational investigation into the potential of aluminum-doped boron nitride nanotubes for hydrogen storage

Mehdi Noura
Department of Physics, University of Zabol, Zabol

Abbas Rahdar
Department of Physics, University of Zabol, Zabol

S. Maryamdokht Taimoory
Department of Chemistry and Biochemistry, University of Windsor

John J. Hayward
Department of Chemistry and Biochemistry, University of Windsor

S. Iraj Sadraei
Department of Chemistry and Biochemistry, University of Windsor

See next page for additional authors

A theoretical first principles computational investigation into the potential of aluminum-doped boron nitride nanotubes for hydrogen storage

Mehdi Noura[†1], Abbas Rahdar[1†*], S. Maryamdokht Taimoory[†2], John J. Hayward[2], S. Iraj Sadraei[2], John F. Trant[2*]

[†] These authors contributed equally to this work.

[1] Department of Physics, University of Zabol, Zabol, P. O. Box. 35856-98613, Islamic Republic of Iran

[2] Department of Chemistry and Biochemistry, University of Windsor, Windsor, ON, N9B 3P4, Canada

* Corresponding Authors

Email addresses: a.rahdar@uoz.ac.ir; j.trant@uwindsor.ca

Corresponding author for the editorial office:

Dr. John F. Trant

Fax Number: 1-519-973-7098

Phone number: 1-519-253-3000 extension 3528

Abstract

Hydrogen storage remains a largely unsolved problem facing the green energy revolution. One approach is physisorption on very high surface area materials incorporating metal atoms. Boron nitride nanotubes (BNNTs) are a promising material for this application as their behaviour is largely independent of the nanoscopic physical features providing a greater degree of tolerance in their synthesis. Aluminum doping has been shown to be a promising approach for carbon nanotubes but has been underexplored for BNNTs. Using first principles density functional theory, the energetics, electronics and structural impacts of aluminum adsorption to both zigzag and armchair polymorphs of BNNTs was investigated along with their potential capacity to adsorb hydrogen. The fine atomic structural and electronic details of these interactions is discussed. We predicted that in an ideal situation, highly aluminum-doped armchair and zigzag BNNTs could adsorb up to 9.4 and 8.6 weight percent hydrogen, well above the United States Department of Energy targets marking these as promising materials worthy of further study.

Keywords:
First principles density functional theory, boron nitride nanotubes, aluminum doping, hydrogen storage, partial density of states

1. Introduction

Human activity is resulting in ever growing energy needs, and this has translated to ever greater levels of carbon dioxide emissions;[1] latest estimates suggest an annual output of nearly 40 billion tonnes,[2] corresponding to the fastest rising levels of atmospheric CO_2 in measured geologic history to almost 390 ppm, up from 280 ppm in 1850.[3] Along with other greenhouse gases, this rise has been responsible for the almost 1.1 °C increase in average global surface temperature since the late 19th century. Warming has accelerated in the past 35 years: 16 of the 17 warmest years have been recorded since 2001. Changes have been extreme enough that we have clearly entered a new geologic epoch defined by human activity.[4] Further global warming will result in consequences regarded as "between bad and catastrophic."[3] Continuing use of fossil fuels is an existential threat to humanity. Decarbonization of the economy is desperately required. Fortunately, decarbonization is economically viable, and renewable and nuclear power could be used to replace current carbonaceous power generation, but transport remains a technological challenge: fossil fuel-based transportation was liable for 23% of global CO_2 emissions in 2014, with road transport the largest contributor at 20% of total emissions.[1, 5] A portable energy carrier is essential to overcome this remaining technological challenge to a green energy future.

Hydrogen is an ideal candidate, but its physical storage remains challenging: liquefaction of hydrogen requires heavy high-pressure tanks, resulting in inefficient storage because the energy density is low. New technologies that exploit chemical interactions between H_2 and porous materials show promise to reach the United States Department of Energy ultimate threshold target of 6.5 weight percent (wt%) storage of hydrogen.[6] To achieve this target, hydrogen storage devices should be composed of very light elements with a large surface area. Carbon nanotubes (CNTs) are the archetypal material due to their large specific surface area allowing for easy adsorption of gases. Unfortunately, hydrogen gas shows poor affinity for a pure carbon surface restricting loading to 0.1-0.5 wt% at ambient temperature and 30 bar.[7] Without induced polarity and/or defects, there are few opportunities for molecular interaction between the surface and the hydrogen molecule.[8] Alternatively one can employ very polar bonds, and although systems like alkali hydrides do have very high hydrogen storage capacity,[9] the reactivity and high costs associated with stoichiometric production and storage makes them potentially economically unfeasible on scale,[10] although efforts are continuing.[11] Combining these two concepts by employing metal-

doped carbon nanotubes,[12] or MOFs[13] has been fruitful, although fraught with pitfalls due to errors in measurement and interpretation.[14]

Boron nitride nanotubes (BNNTs) are an alternative light-weight material which have been proposed as useful alternatives to CNTs since their first synthesis.[15] Due to their electronic homogeneity, the properties of BNNTs are independent of the diameter or chirality of the tube,[16] and their chemical inertness coupled with their excellent thermal stability makes them extremely promising materials for hydrogen storage,[17] potentially more useful than CNTs,[18] but likely doped rather than as pristine BNNTs.[19] The experimental evidence is compelling: in 2002 Ma *et al.* measured that their multiwall bamboo-like BNNTs stored up to 2.6 wt% hydrogen at room temperature;[20] Tang and coworkers reported "collapsed" BNNTs (tripling the surface area from 255 to 790 m^2/g) can absorb 4.2 wt% hydrogen at room temperature.[21] Doping with other elements improves this markedly: Chen has reported that incorporating 4% oxygen atoms can increase hydrogen capacity to 5.7 wt%.[22] These results and the contributions of others have stimulated a wealth of computational simulations aiming to predict the hydrogen capacity of variously doped nanotubes including with Rh, Ni and Pd;[23] Ti;[24]; carbon;[25] Pt;[26] Ce;[27] Ca;[28] Na;[29]; Li;[30]; K;[31] and the capacity of differentially occupied endohedral $B_{16}N_{16}$.[32] All of this work has been well reviewed recently.[33]

Aluminum is highly promising dopant,[34] although the studies are all computational at this time,[35] we could find no experimental reports examining the hydrogen adsorption properties of this material; however doping $NaAlH_4$ with CNTs has been shown to increase the kinetics of the decomposition of the salt to provide H_2.[36] It is an attractive material as the cost is low and aluminum atoms are predicted to greatly facilitate hydrogen binding to the surface of carbon nanotubes.[37] Al-doped BNNTs (**BNNT-Al**) have been investigated computationally for hydrazine,[38] hydrocyanic acid,[39] and mercaptans[40] along with other gases.[41] However, hydrogen storage has surprisingly not been explored in detail. One reason is the difficulty in preparing these systems experimentally as metallic aluminum is highly susceptible to oxidation, so the promise of direct functionalization is low. However, this could be addressed in the right environment, and insight into the behaviour of an idealized system would provide insight into design of hydrogen-storage materials. Zhang and coworkers provided a preliminary report on the possible bond length and adsorption energy of hydrogen on a rarer (6,6) BNNT polymorph, but did not expand on the factors responsible for the predicted geometries.[42] In this report we discuss the hydrogen storage

potential of both the experimentally accessible zigzag (5,0)[43] and armchair (3,3)[44] BNNT polymorphs by using first principles methods with various numbers of aluminum atoms and various numbers of hydrogen atoms present.

2. Computational Methods

All calculations were performed using the Born-Oppenheimer approximation within the framework of density functional theory (DFT) and employing the plane-wave basis set and pseudopotentials as employed in the Quantum ESPRESSO package implemented on Compute Canada.[45] Self-consistency calculations following the Kohn-Sham formalism[46] were used for solving the single particle equations with Quantum ESPRESSO. For all DFT calculations we used the local density approximation (LDA) in its Ceperley and Alder (CA) form as approximated by Perdew-Zunger (PZ) for the exchange-correlation functional (XC). To better approximate the relativistic effects, the radial Dirac equations derived from the scalar relativistic approximation (SRA) were used.[47] Configurations of $2s^2 2p^1$ of B, $2s^2 2p^3$ of N, $3s^2 3p^1$ of Al and $1s^1$ of H atoms were treated as the relevant valences using the USPP pseudopotentials generated for LDA based functionals implemented in Quantum ESPRESSO.

To accurately model long nanotubes, a periodic boundary condition was used along the super cell nanotube axis for each nanotube, with the dimensions of simulated super cells ranging from 28×28×37 Å^3 for the smallest systems to 46×46×37 Å^3 for the largest systems. To optimize the geometries of nanotubes, the wave functions were expanded in a plane wave basis set with a kinetic energy cutoff of 70 Ry. Calculations were performed at the center of the Brillouin zone (Γ–point only). To ensure convergency and to select the appropriate value of both the cutoff energy and the Brillouin zone, an initial series of self-consistent field (SCF) calculations, varying either the cutoff energy or the number of k-points was performed. Initial geometries of nanotubes placed at the Γ–point were optimized using the conjugate gradient (CG) method with a convergence criterion of 1×10^{-4} eV for total nanostructure energy.[48] An additional convergence criterion of 0.09 eV/Å was imposed for each force component.

The zigzag (5,0) and armchair (3,3) BNNT polymorphs were selected for detailed study. These two nanotubes have different chirality, but almost identical diameters. A large supercell with four units and growth along the z axis was used. This is large enough to minimize interactions between atoms. In order to remove the effect of dangling bonds at the end of the nanotubes, 10 and 12 hydrogen atoms are added to the (5,0) and (3,3) BNNTs, respectively.

The calculated binding energy, E_b, of an Al atom doped onto the hollow site of a BNNT was determined according to Equation 1, where m indicates number of Al atoms and $E_{TOT}(\mathrm{BNNT})$, $E_{TOT}(m\mathrm{Al})$ and $E_{TOT}(m\mathrm{Al@BNNT})$ represent the total energies of a pure BNNT, one or more free Al atoms, and the Aluminum-decorated BNNTs respectively.

$$E_b(\mathrm{Al}) = \left[\frac{[E_{TOT}(\mathrm{BNNT}) + mE_{TOT}(\mathrm{Al})] - E_{TOT}(m\mathrm{Al@BNNT})}{m}\right] \quad \textbf{(Equation 1)}$$

The adsorption energy per H_2 molecule was calculated using Equation 2, where $E_{TOT}(m\mathrm{Al@BNNT})$ is the total energy of the mAl@BNNT and $E_{TOT}(n\mathrm{H_2})$ and $E_{TOT}(n\mathrm{H_2} \cap m\mathrm{Al@BNNT})$ are the total energies of the corresponding optimized structures of the free hydrogen molecules and the adsorbed structures.

$$E_b(\mathrm{H_2}) = \left[\frac{E_{TOT}(\mathrm{mAl@BNNT}) + E_{TOT}(n\mathrm{H_2}) - E_{TOT}(n\mathrm{H_2} \cap \mathrm{mAl@BNNT})}{n}\right] \quad \textbf{(Equation 2)}$$

The partial density of states was calculated using a dense-grid calculation on the initially SCF predicted geometry applying PWgui[49] and postprocessed and plotted using the XCrySDen package.[50]

The charge transfer induced by the absorbed H_2 molecules on the BNNT were obtained by the Mulliken population analysis of $\boldsymbol{m}$**Al@BNNT** and $\boldsymbol{n}\mathbf{H_2} \cap \boldsymbol{m}$**Al@BNNT** *versus* the initial BNNT structure. The electric dipole moment for BNNTs was determined using the UB3LYP functional within the Gaussian09 package implemented in Compute Canada.[51]

3. Results and discussion

3.1 Geometry of the mono-Al decorated Boron-Nitride nanotube (*1*Al@BNNT)

We initially modeled and studied the structural details of both zigzag (5,0) and armchair (3,3) BNNTs and their ***1*Al@BNNT** complexes where a single Al atom is adsorbed at the center of a BN(B_3N_3) hexagon using the reported structure of Al doped CNT as a starting point for generating the structures (Figure 1).[34]

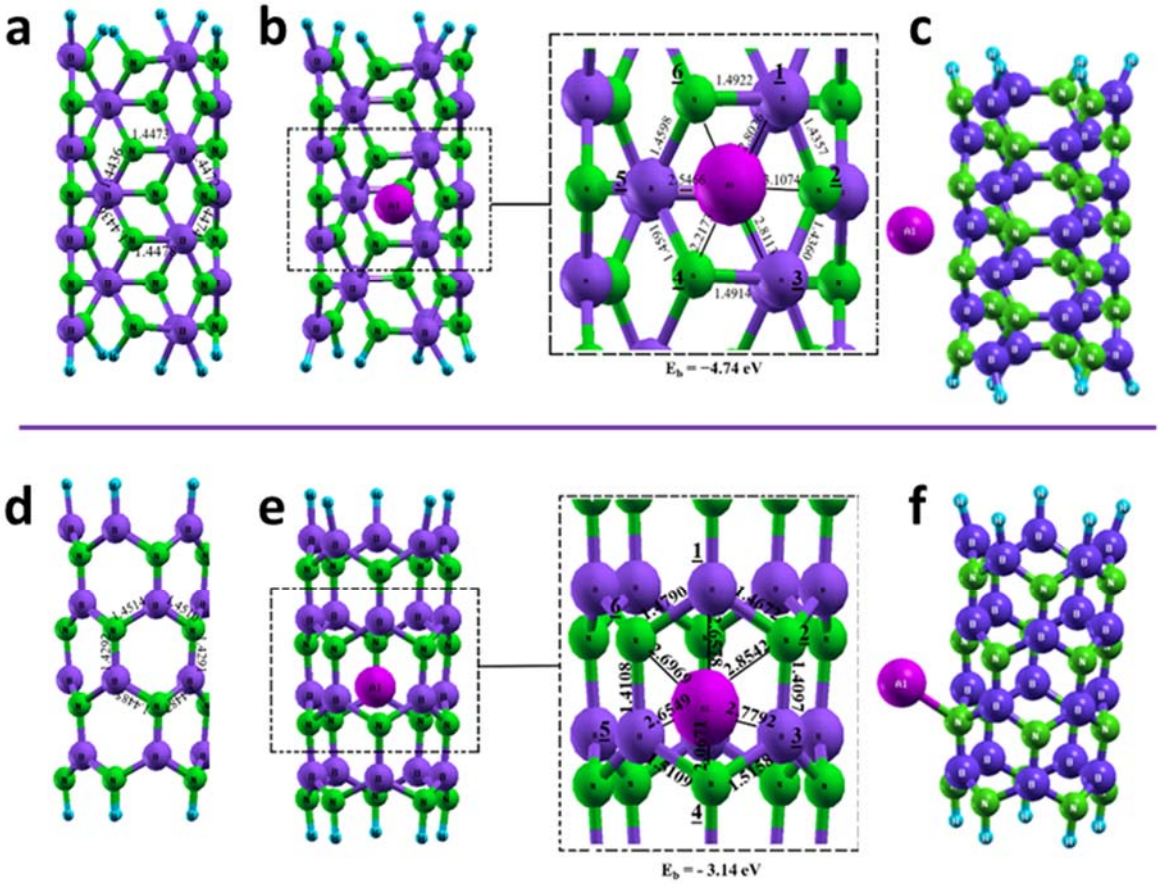

Figure 1. The optimized geometry and the calculated binding energies of **a) BNNT(3,3)**; **b) *1*Al@BNNT(3,3)** with an expansion showing distances to the labelled nearest neighbor atoms, and the binding energy; **c)** side-view of the same; **d) BNNT(5,0)**; **e) *1*Al@BNNT(5,0)** with an expansion showing distances to the labelled nearest neighbor atoms, and the binding energy; and **f)** side-view of the same.

Consistent with experiment,[52] our calculations show that the (5,0) zigzag nanotube is the energetically preferred polymorph. The predicted structures show B−N bond lengths between 1.44 – 1.45 Å and 1.43 – 1.45 Å for **BNNT(3,3)** and **BNNT(5,0)** respectively, again in good agreement with the experimental value of 1.45 Å (Table 1).

The fully optimized ***1*Al@BNNT** geometries show that adsorption disrupts the symmetry of these structures, lengthening the B−N bond length (Table 1). In ***1*Al@BNNT(3,3)**, the aluminum atom does not sit in the middle of the hollow, as it forms a stronger interaction with two of the nitrogen atoms (2.20 and 2.21 Å) than the third (3.10 Å, Table 2). In ***1*Al@BNNT(5,0)**, the aluminum binds much more tightly to one of the nitrogen atoms (2.07 Å) compared to the other two (2.70 and 2.85 Å, Figure 1f). The aluminum of course sits closer to N than B as the electron

density localizes around the more electronegative N atom than the B resulting from the formation of a partially polar covalent bond between Al and N (Table 2, Table S1 and S2).

Table 1. The predicted neighboring B−N distances of the pure and mono-aluminum-doped BNNTs (Å).

	B1-N2	**N2-B3**	**B3-N4**	**N4-B5**	**B5-N6**	**N6-B1**
BNNT(3,3)	1.45	1.45	1.45	1.45	1.44	1.44
***1*Al@BNNT(3,3)**	1.49	1.44	1.44	1.49	1.46	1.46
BNNT(5,0)	1.45	1.43	1.45	1.45	1.43	1.45
***1*Al@BNNT(5,0)**	1.47	1.41	1.52	1.51	1.41	1.48

Table 2. The predicted neighboring Al-B and Al-N bond lengths in the doped BNNTs (Å)

	Al-B1	**Al-N2**	**Al-B3**	**Al-N4**	**Al-B5**	**Al-N6**
1Al@BNNT(3,3)	2.80	3.11	2.81	2.22	2.55	2.21
1Al@BNNT(5,0)	2.66	2.85	2.78	2.07	2.65	2.70

The calculated binding energy (E_b) is −4.74 eV/Al-atom for ***1*Al@BNNT(3,3)**, which is 1.6 eV/Al-atom larger than for ***1*Al@BNNT(5,0)**. This stronger bonding to the armchair (3,3) BNNT is largely due to increased torsional strain in this polymorph that results from the higher curvature of the surface leading to more reactive B-N bonds, and a more nucleophilic nitrogen. Curvature impacts not only the thermodynamics of adsorption, but has also been implicated in determining the differential kinetics and the observed structural distortions.[53] However, the adsorption process for both systems is highly favorable, and at > 0.5 eV is best described as chemisorption rather than a purely physical process.

3.2 Partial density of states properly describes the binding mode

The partial density of states (PDOS) of the systems were determined using the computed self-consistent potential predicted for both the **BNNTs** and the ***1*Al@BNNTs** with the Fermi level, E_F , set to zero (Figure 2). In the pristine BNNTs, the major contributor to the valance band comes from N-2p, while the major contributor to the conduction band comes from B-2p, although the

details do differ between the two BNNT geometries. Upon Al-adsorption, both bands shift to lower energy states indicating an increase in stability of the BN scaffold.

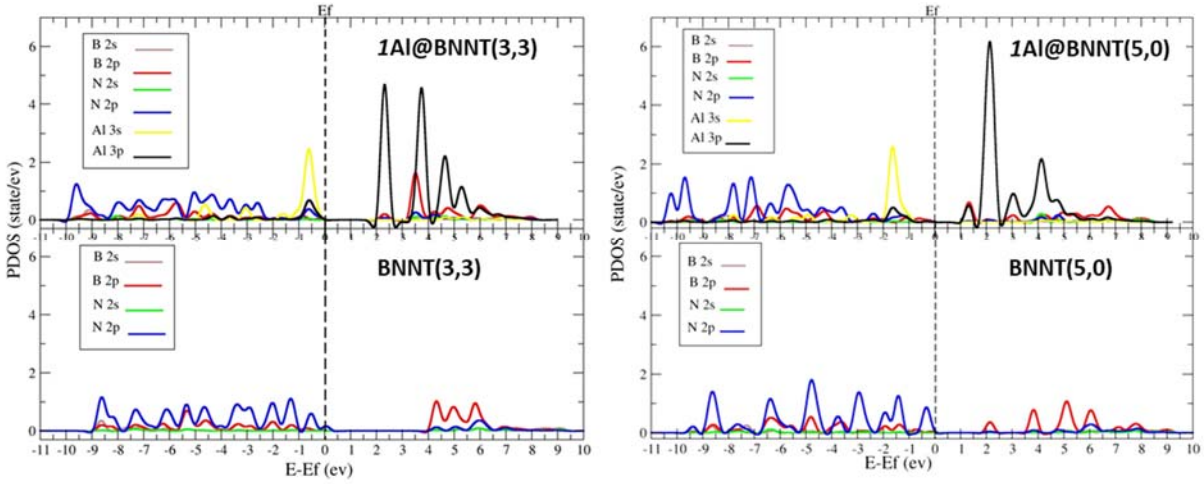

Figure 2. Partial density of state (PDOS) of the pristine and aluminum-doped BNNTs. The perpendicular dashed lines denote Fermi levels (set to 0).

A strong hybridization is established between the Al-3s and 3p orbitals and the B-2p and N-2p orbitals of the BNNTs. The Al 3s orbitals shift negative (Figure 3) mainly occupying a single energy level suggesting they do not interact significantly with the B and N orbitals. However, the symmetry effects of the two systems come into play with the splitting in the energy levels of the Al 3p orbitals. In both cases the partially occupied 3p orbital of aluminum metal is emptied on complexation as the electrons occupy the higher energy hybridized orbitals states. This involves a significant charge transfer: the charge of Al falls by 0.579 e and 0.509 e upon association to **BNNT(3,3)** and **BNNT(5,0)** respectively (see Tables S1 and S2 Supporting Information). The Al-3p orbital splits into three peaks due to the electric field generated by the BNNTs nanotubes. In ***1*Al@BNNT(3,3)**, there are two major (2.2 and 3.6 eV), and one lesser population in the conductance band, while the population at 2.2 eV dominates the conductance band for ***1*Al@BNNT(5,0)**. The fact that this effect is stronger for the **BNNT(3,3)**, than **BNNT(5,0)** also helps explain the better binding energy in the former. Furthermore, Al doping reduces the band gap by 2.448 eV and 1.60 eV for **BNNT(3,3)**, and **BNNT(5,0)** respectively.

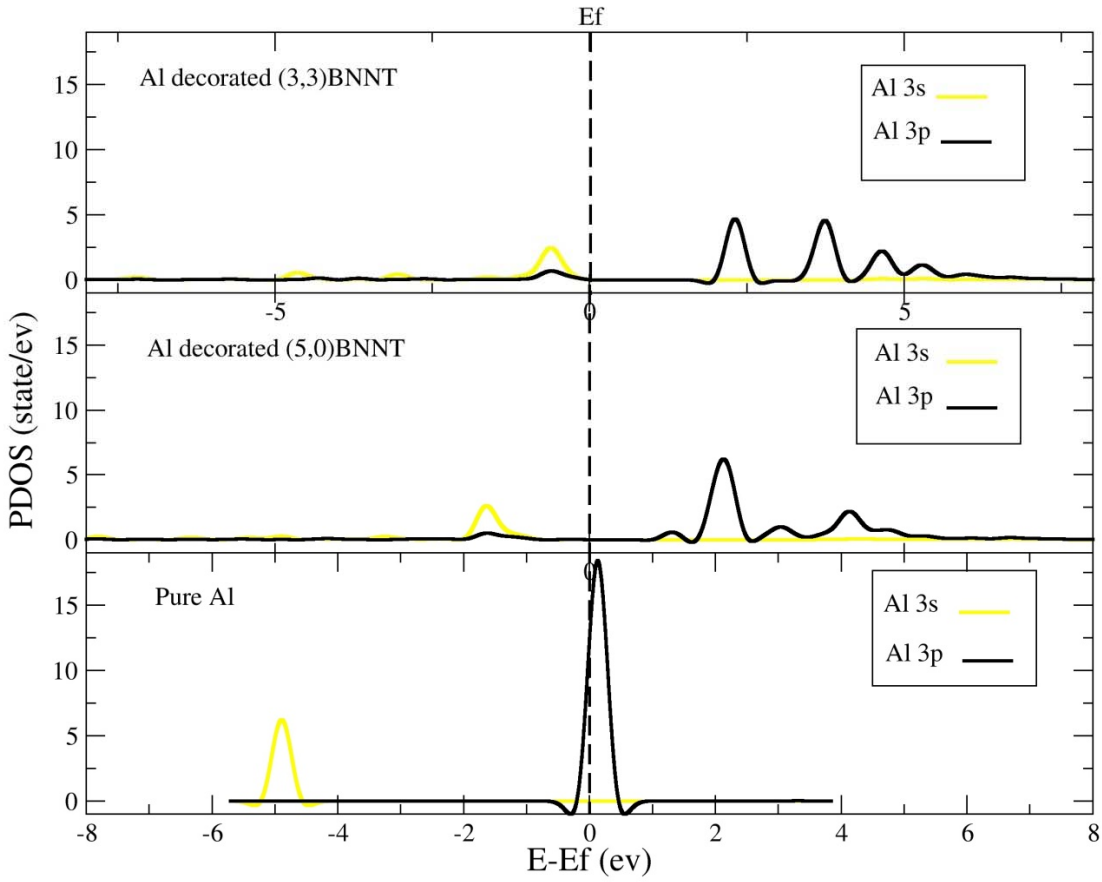

Figure 3. PDOS of aluminum, ***1*Al@BNNT(5,0)** and ***1*Al@BNNT(3,3)**.

These results are consistent with the well-established observation that BNNTs are n-type semiconductors. During adsorption, the Al is the electron donor to the BNNT's electron acceptor. The charge transfer allows electrons in the valence band to move freely, producing an electric field that leads to stronger and closer interactions with hydrogen molecules possibly enhancing loading.

These results could explain the Mulliken atom charge difference, the observed charge transfer, and the induced dipole moment. The predicted charge transferred between the Al donor and nanotube acceptors ($Al^{\delta+}\cdots N^{\delta-}$—B) affects atoms several bonds away and induces an electric field and in turn changes the magnitude and direction of the dipole moment vector of **Al@BNNT** relative to **BNNT**. The already polar B-N bonds in **BNNT(5,0)** become far more polar, while the previously non-polarized B-N bonds in **BNNT(3,3)** become polar.

The dipole moment of **BNNT(5,0)** is 6.28 D and is aligned along the main axis of the nanotube. As the Al atom approaches, the dipole vector reorients towards the Al atom along the

Al−N interaction, with a concurrent increase in magnitude to 9.88 D. Association rotates the vector almost 90º and the precise angle arises based on the preference of the Al to interact primarily with a single nitrogen atom. In contrast to the polar zigzag polymorph, the **BNNT(3,3)** armchair form is relatively non-polar with only a small dipole moment of 0.12 D: despite the polarity of the nanotube's B−N bonds, the symmetry and geometric arrangement of these bonds is such that the bond dipole moments are overall aligned in opposition to each other and thus resulting in a molecule with no net dipole moment. Adsorption of Al disrupts this symmetry resulting in a significant increase in the magnitude of the dipole moment vector to a value of 3.77 D, greatly increasing the polar nature of the surface.

The total charge density contour plots for the Al-decorated systems were calculated (Figure 4, Figure S1). The charge density is primarily located around the nitrogen atoms. Al adsorption perturbs the charge distribution, breaking the symmetry of the contour lines, however it is spread over the local area and not all localized on the nitrogens interacting with the aluminum. This rearranged density overlaps between the Al and the BNNT highlights that this is a chemical reaction, not just physical adsorption. The Al becomes part of the molecule partaking in the electronic charge flow between the atoms of the BNNT tube and the Al atom. The electron density within the tubes varies based on geometry: in ***1*Al@BNNT(3,3)** the symmetry of the system and electron density around the nearby nitrogen atoms is only partially disturbed, though the electron density within the tube shifts towards the aluminum-bound side (the greater disruption occurs out-of-plane with the third nitrogen of the ring that doesn't interact equally with the Al center). For ***1*Al@BNNT(5,0)** the local symmetry is greatly disturbed as the aluminum favors one of the nitrogens of the six-membered ring more than the other two and this charge delocalization assists the adsorption process. The already polar system is further disturbed with electron density shifting towards the aluminum side.

Aluminum chemisorption changes the electronic structure of the local BNNT and this is expected to have an impact on the affinity for molecular hydrogen.

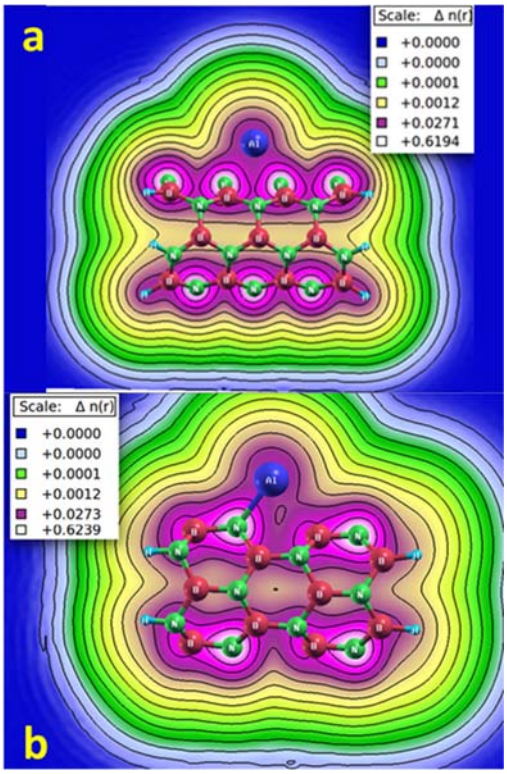

Figure 4. Charge density contour plot of **a) *1*Al@BNNT(3,3)** and **b) *1*Al@BNNT(5,0)** from a side-on view.

3.3. Adsorption of the first hydrogen molecule onto *1*Al@BNNT(3,3) and *1*Al@BNNT(5,0)

The optimized geometries of a single H_2 molecule located near the adsorbed Al atom were modelled and the structural evaluation were made following the known chemical and electronic character of H−Al and H−H bonds (Figure 5).

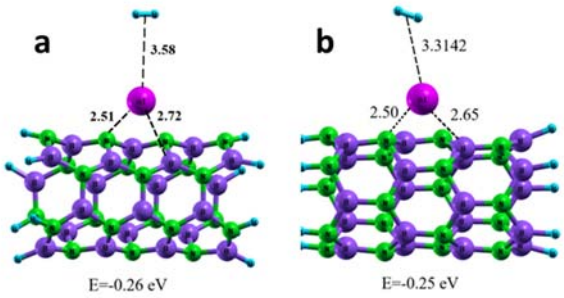

Figure. 5. The first principle optimized geometry of a) ***1*H$_2$⋂*1*Al@BNNT(3,3)** and b) ***1*H$_2$⋂*1*Al@BNNT(5,0)**.

The first observation is that the hydrogen interacts with the aluminum atom, not the BNNT. Hydrogen adsorption changes the distance between Al and the centroid of the BNNT: it increases from 2.61 Å in ***1*Al@BNNT(3,3)** to 2.62 in ***1*H_2⋂*1*Al@BNNT(3,3)**; but decreases from 2.61 Å ***1*Al@BNNT(5,0)** to 2.57 Å for ***1*H_2⋂*1*Al@BNNT(5,0)**. The H_2 molecule sits 3.58 Å and 3.31 Å from the Al atom ***1*H_2⋂*1*Al@BNNT(3,3)** and ***1*H_2⋂*1*Al@BNNT(5,0)** respectively. Binding also activates the hydrogen: the H-H bond length increases from 0.74 in molecular hydrogen to 0.77 Å when bound to either BNNT system, this is much larger than the increases observed for binding to alkali-doped carbon nanotubes (0.748-0.756 Å) demonstrating the good affinity to the ***1*Al@BNNT**.[54] The interaction has a weak van der Waals character (H-H and H-Al) which is easily broken as the binding energy is only -0.26 eV/H_2 and -0.25 eV/H_2 for ***1*H_2⋂*1*Al@BNNT(3,3)** and ***1*H_2⋂*1*Al@BNNT(5,0)** respectively. For reversible hydrogen storage at ambient conditions, the desirable H_2 binding energy should be in the range of 0.20-0.40 eV/ H_2;[7b] these materials appear suitable.

Importantly, the charge density plots provide further insight into this interaction (Figure S2). The hydrogen molecule lies parallel to the nanotube axis, meaning the electron cloud also lies parallel to the axis. However, as there is no overlap between the electron clouds of the hydrogen molecule and the ***1*Al@BNNT**, this is a clear case of physisorption. The interaction is strong enough that we do disturb the electron density within the tube though and increase the polarity of the system. The partial density of state (PDOS) analysis supports these contentions (Figure 6). In both ***1*H_2⋂*1*Al@BNNT(3,3)** and ***1*H_2⋂*1*Al@BNNT(5,0)**, the H 1s orbital lies well below the Fermi level, remaining intact with no meaningful overlap with either the Al 3s or 3p orbitals again indicating no strong chemical interaction between the two systems. The Al 3p orbitals reorganize very slightly for ***1*H_2⋂*1*Al@BNNT(5,0)** showing that binding does have an impact on the electronic structure of the atom, but again, it is very minor. The weakness of this interaction is emphasized by the very small effect it has on the band gap energy, decreasing that of ***1*H_2⋂*1*Al@BNNT(3,3)** by 0.16 eV, and increasing that of ***1*H_2⋂*1*Al@BNNT(5,0)** by 0.01 eV relative to the ***1*Al@BNNT** systems. The weak binding effect is due almost entirely to electrostatic interactions between the aluminum atom and the now polarizing hydrogen bond, essential for the rapid association dissociation processes that must occur in any hydrogen storage medium.

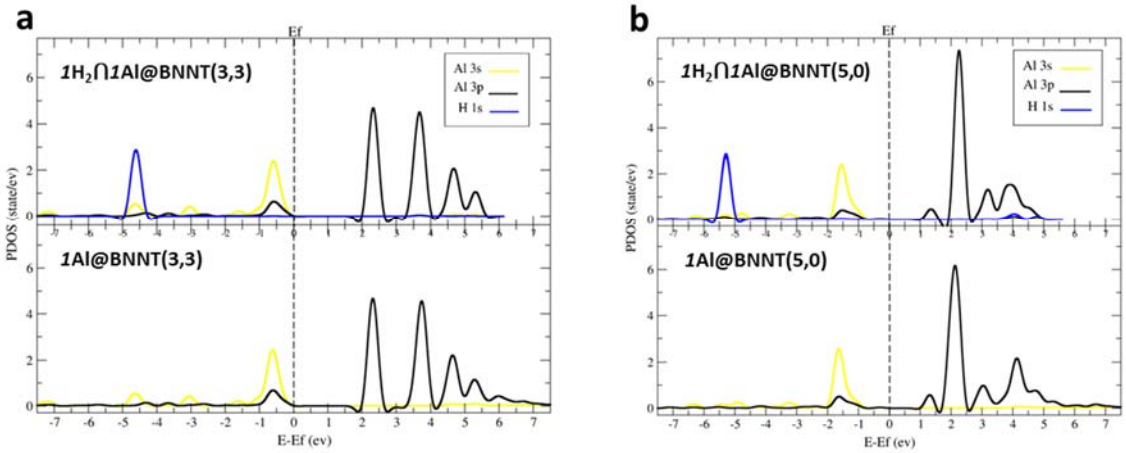

Figure 6. The plotted PDOS of the Al atom both before and after H_2 adsorption for both a) **1H₂⋂*1*Al@BNNT(3,3)** and b) **1H₂⋂*1*Al@BNNT(5,0)**.

According to the calculated Mulliken charge, the Al atom becomes more polarized during the adsorption of the H_2 molecule on BNNT-1Al as the positive charge on the Al atom increases from 0.570 *e* to 0.572 *e* for ***1*H₂⋂*1*Al@BNNT(3,3)** and from 0.509 *e* to 0.515 *e* for ***1*H₂⋂*1*Al@BNNT(5,0)**. Aluminum binding significantly increased the dipole moment, and shifted the direction of the vector, for both BNNTs, but hydrogen adsorption is a far less drastic process increasing the dipole moment of ***1*H₂⋂*1*Al@BNNT(3,3)** to 3.81 D from 3.77 D, and decreasing that of ***1*H₂⋂*1*Al@BNNT(5,0)** to 9.73 D from 9.88 D for the parent ***1*Al@BNNT(5,0)**.

3.4. Adsorption of multiple H_2 molecules onto the surface

To analyze the hydrogen storage capacity of these Al-decorated BNNTs, the geometries of ***1*Al@BNNT(3,3)** and ***1*Al@BNNT(5,0)** coordinated with 1 to 7 H_2 molecules were investigated using plane wave DFT (Figures 7 and 8). To initially model those higher order assemblies, the n^{th} H_2 molecules were iteratively added to the simulated geometries of (***n-1)*H₂⋂*1*Al@BNNT(3,3)** and (***n-1)*H₂⋂*1*Al@BNNT(5,0)** and after each addition the structures were relaxed. The first hydrogens interact directly with the aluminum center; in the case of ***7*H₂⋂*1*Al@BNNT(3,3)** all the hydrogens can be accommodated within this first coordination sphere, while for ***6*H₂⋂*1*Al@BNNT(5,0)** and above, one or more hydrogens is located more distantly from the aluminum. The calculated average adsorption distance, average H_2 bond length, the degree of

charge localized on Al, and the predicted binding energy per H_2 molecule adsorption are summarized in Tables 3 and 4.

The electronic character of the involved atoms changes as the number of hydrogen atoms increases. To improve affinity as the number of ligands increases, the aluminum atom transfers more electron density to the BNNT to compensate for the increased donation from the hydrogen molecules. The overall charge on the Al atom starts at +0.57 in ***1*Al@BNNT(3,3)**, and shifts rapidly to essentially neutral upon the addition of the third hydrogen molecule. This also flips the direction of the predicted dipole moment and is clearly a boundary condition. The effect is far more subtle on ***1*Al@BNNT(5,0)** as the charge slowly decreases from an initial value of 0.509 to 0.440 at ***6*H_2⋂*1*Al@BNNT(5,0)**. This is the starkest contrast in behaviour differences between the two systems, and we recalculated these values multiple times using slightly different methods but always identified the same trend. The electron density increase on the Al is compensated for by a delocalized decrease on the BNNT in the case of ***n*H_2⋂*1*Al@BNNT(3,3)**, $n \geq 3$.

As noted, the H_2 binding energy should ideally be between 0.2 and 0.4 eV/H_2 to be good enough to adsorb a significant amount of hydrogen while at the same time allowing for easy desorption so that it can be used. Capacity would be increased if binding energy remains favorable as additional hydrogen molecules are added: for context, the average binding energy of 1-8 H_2 for potassium-doped (5,0) and (3,3) BNNTs was on the low end at 0.09 to 0.22 eV suggesting that binding might not be sufficient with these alkali-metal doped systems.[31] In this study, the binding energy largely falls within the desired window: 0.233 to 0.33 eV/H_2 for ***n*H_2⋂*1*Al@BNNT(3,3)**, n = 1-7; and 0.25-0.41 eV for ***n*H_2⋂*1*Al@BNNT(5,0)**, n = 1-7. Our data predicts that 5-6 hydrogen molecules is the probable number adsorbed to ***1*Al@BNNT**; this quantity provides the balance between the weak synergistic interaction of the H_2 molecules to a single Al atom and the presence of coulomb repulsion. Mahendran reported that four hydrogen atoms (E_b= 0.214 eV/H_2) was the maximum absorbable per aluminum atom on a high-density aluminum-doped carbon nanotube (low density doping resulted in an extremely strong, and storage-wise useless chemisorption of 2.01 eV/H_2).[34] Six hydrogen molecules is clearly an improvement.

This analysis suggests that low-level aluminum doping of BNNTs would be effective for turning these into high capacity hydrogen storage vessels with binding energies in the desired window to allow for fast and ready adsorption of hydrogen, followed by simple desorption at ambient temperatures, precisely the qualities needed for next generation hydrogen storage devices

overcoming the limitations of current technologies.[10, 55] However higher levels of aluminum doping might be a better representative of an experimentally attainable system.

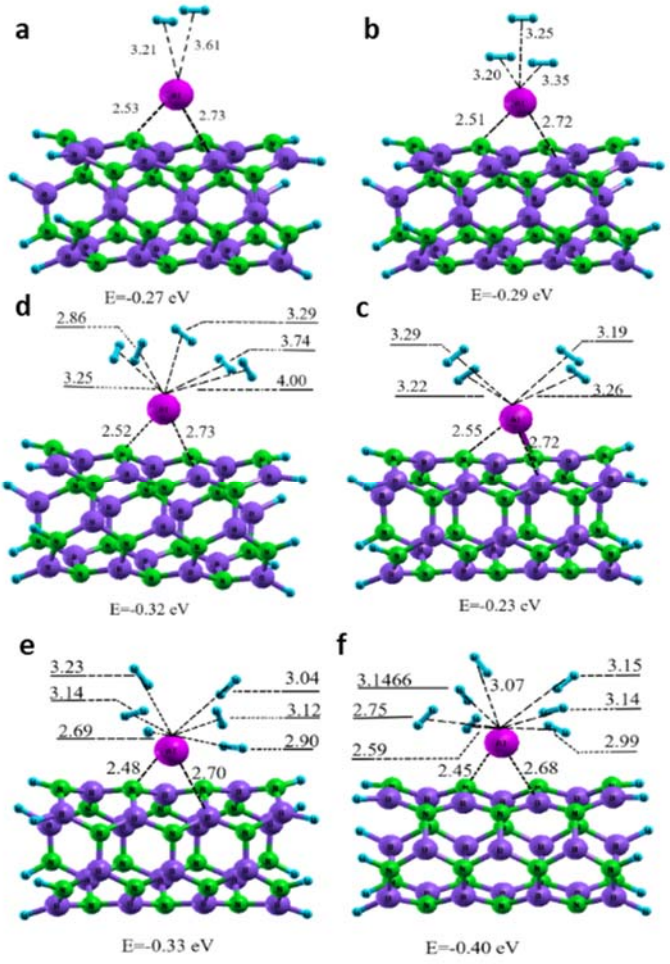

Figure 7. Al-decorated **(3,3) BNNT** with 2-7 molecules adsorbed. Al atom is decorated at the center of the hexagonal (H site). Dashed lines represented the distance from Al to center of mass of H_2(Al-H_2). All distances are given in Å.

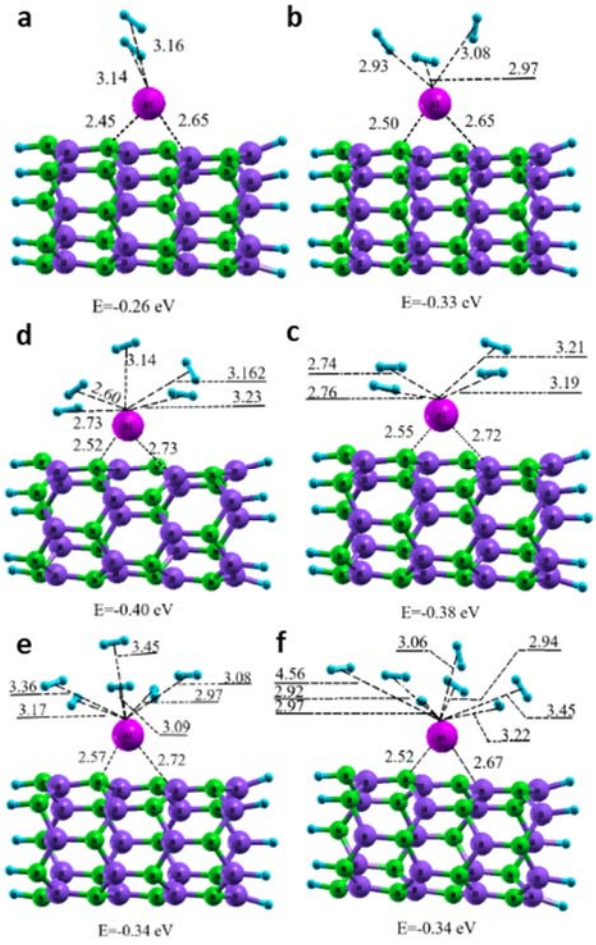

Figure 8. Al-decorated **(5,0) BNNT** with 2-7 H_2 molecules adsorbed. Al atom is decorated at the center of the hexagon (H site). Dashed lines represented the distance from Al to center of mass of H_2(Al-H_2). All distances are given in Å.

Table 3. The Mulliken charges (a.u.) on Al atom, the dipole moment(D), the calculated bond length (Å), and binding energy of H_2 (eV/H_2) on (3,3) Al-BNNT.

System	E_b(eV)	$\bar{d}_{Al-B}$ (Å)	$\bar{d}_{Al-N}$(Å)	$\bar{d}_{Al-H_2}$(Å)	$\bar{d}_{H-H}$(Å)	$\text{Charge}_{\text{Al}}$	Dipole	$\bar{d}_{B-N}$(Å)
$0H_2$	-------	2.72	2.51	------	------	+0.57	------	1.4620
$1H_2$	-0.267	2.72	2.52	3.58	0.766	+0.57	3.82	1.4623
$2H_2$	-0.277	2.73	2.53	3.41	0.767	+0.58	4.03	1.4612
$3H_2$	-0.290	2.72	2.52	3.26	0.766	-0.018	4.22	1.4619

$4H_2$	-0.233	2.73	2.55	3.29	0.768	-0.091	2.26	1.4632
$5H_2$	-0.322	2.74	2.53	3.30	0.767	-0.034	4.78	1.4610
$6H_2$	-0.330	2.71	2.49	3.26	0.771	+0.15	5.59	1.4637
$7H_2$	-0.400	2.68	2.46	2.54	0.774	+0.14	5.69	1.4659

Table 4. The calculated bond length (Å), Mulliken charges (a.u.) on Al atom and the predicted binding energy of H_2 (eV/H_2) on (5,0) Al-BNNT.

System	E_b(ev)	$\bar{d}_{Al-B}$	$\bar{d}_{Al-N}$	$\bar{d}_{Al-H_2}$	$\bar{d}_{H-H}$	$Charge_{Al}$	Dipole	$\bar{d}_{B-N}$
$0H_2$	-------	2.68	2.54	------	------	+0.509	9.88	1.4655
$1H_2$	-0.250	2.65	2.50	3.31	0.781	+0.515	9.74	1.4625
$2H_2$	-0.266	2.65	2.45	3.14	0.769	+0.515	9.92	1.4628
$3H_2$	-0.331	2.65	2.50	2.92	0.772	+0.485	9.71	1.4640
$4H_2$	-0.382	2.66	2.51	2.75	0.772	+0.517	10.36	1.4762
$5H_2$	-0.406	2.70	2.55	3.14	0.773	+0.490	10.83	1.4651
$6H_2$	-0.346	2.73	2.57	3.36	0.769	+0.440	11.49	1.4644
$7H_2$	-0.346	2.68	2.53	3.31	0.771	+0.467	10.86	1.4647

3.5 Loading-up, effect of poly aluminum doping on hydrogen adsorption on BNNTs

The optimized per-aluminated systems for each BNNT architecture were determined to be ***6*Al@BNNT(3,3)** and ***5*Al@BNNT(5,0)** (Figure 9). The average distance between the Al atoms and the nearest atoms of the B_3N_3 hexagons is 2.61 Å and 2.42 Å for ***6*Al@BNNT(3,3)** and ***5*Al@BNNT(5,0)** respectively, which is 0.1 Å greater and 0.12 Å less respectively than the distances calculated for the monosubstituted BNNTs. The Al atoms do not adopt a structure consistent with bulk Al, as the distance between the atoms is far greater (4.02-4.62 Å) than the Al···Al distance in bulk metal (3.39 Å). The two geometries are consistent with what was seen for

the mono-aluminum system. The highly symmetric **BNNT(3,3)** adsorbs the multiple aluminums broadly symmetrically, just as it did the mono-aluminum. ***5*Al@BNNT(5,0)** of course could not be symmetric, and the distances and positionings of the Al atoms relative to the B−N hexagons differs for each metal-BNNT interaction.

The number and arrangement of Al atoms on the BNNT surface changes the charge distribution and electronic properties of the nanotubes. For example, the UB3LYP calculated charge analysis of ***6*Al@BNNT(3,3)** shows that the three aluminums located over the centroid of hexagonal ring of BNNT (Figure 9) experience greater charge transfer than those directly over the bonds. As the number of aluminum atoms increases the degree of charge transfer to each aluminum atom decreases (Table 5). The increased symmetry of the complex, as expected, decreases the dipole moment of ***6*Al@BNNT(3,3)** to 0.84 D from 3.77 D for ***1*Al@BNNT(3,3)**; but it significantly increases the dipole moment of ***5*Al@BNNT(5,0)** relative to its homologue (13.24 D to 9.88 D) as aluminum addition disrupts the organization of the electron cloud around the BNNT. Peralumination also significantly decreases the strength of the binding interaction between the aluminum and the BNNT, which decreases per atom.

For chemisorption of the metal to be effective, the energy of binding to the BNNT must be competitive, and preferably lower than the cohesive energy of bulk aluminum (3.39 eV/atom).[56] This is not the case for these higher order aluminum systems. That of ***6*Al@BNNT(3,3)** is 1.51 eV/Al while that of ***5*Al@BNNT(5,0)** is 1.80 eV/Al. Functionalization of the tubes will need to be done with caution to make it occur. Alternatively, the likeliest form would involve aluminum clusters on the surface of the BNNT rather than uniformly distributed isolated atoms as modelled in this paper. Investigation of these BNNT-supported Al nanoclusters is currently underway by our team.

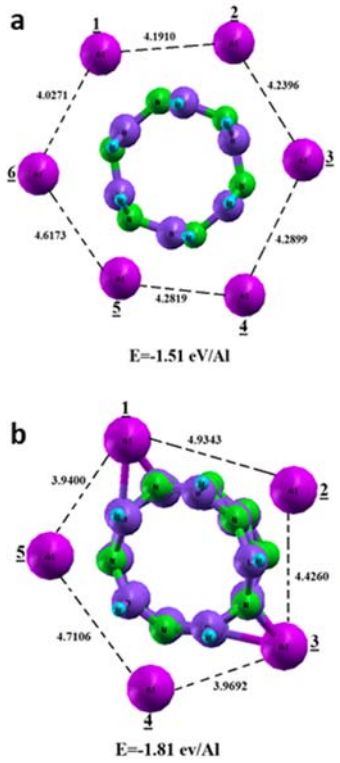

Figure. 9. Top view of the optimized structures of a) ***6*Al@BNNT(3,3)** and b) ***5*Al@BNNT(5,0)**.

Table 5. The calculated Mullikan charge of Al atoms (au)

	Al-1	**Al-2**	**Al-3**	**Al-4**	**Al-5**	**Al-6**	**Dipole moment**
***6*Al@BNNT(3,3)**	0.234	0.077	0.216	0.114	0.201	0.092	0.846
***5*Al@BNNT(5,0)**	0.386	0.410	0.390	0.441	0.423	-	13.244

3.6 Hydrogen adsorption on peraluminated BNNTs

The final analysis of this preliminary study examined the hydrogen adsorption properties of the peraluminated models using our DFT based study. ***5*Al@BNNT(5,0)** can absorb a maximum of thirty H_2 molecules with binding energy of 0.40 eV/H_2, and ***6*Al@BNNT(3,3)** can accommodate thirty-six H_2 molecules with binding energy of 0.39 eV/H_2 (Figure 10). Unlike some studies into Al-functionalized CNTs, the hydrogen atoms do not chemisorb to the surface, but rather remain molecular hydrogen.[37b] In ***36*H$_2$⋂*6*Al@BNNT(3,3)**, addition of the H_2 molecules did not affect the structural reorganization of the Al atoms on the surface wall of nanotube as the Al-BNNT distances do not change due to this process. However, hydrogen adsorption does affect the structure of ***30*H$_2$⋂*5*Al@BNNT(5,0)** where the average Al···Al distance was 3.83 Å compared to 3.66 Å in ***5*Al@BNNT(5,0)**. Moreover, the average distance between the Al and the nitrogen atoms

increased from 2.42 Å in ***5*Al@BNNT(5,0)** to 2.62 Å in ***30*H$_2$⋂*5*Al@BNNT(5,0).** These changes highlight that the aluminum-functionalized zigzag BNNT better accommodates the hydrogen into its native structure than the armchair polymorph which needs to distort considerably from its preferred conformation. This degree of loading translates to 9.45 and 8.61 weight % hydrogen loading for ***36*H$_2$⋂*6*Al@BNNT(3,3)** and ***30*H$_2$⋂*5*Al@BNNT(5,0)** respectively, far above the long-term DOE target of 5.5%.[6] If the synthetic challenges in preparing these systems can be overcome, aluminum-functionalized BNNTs may prove useful storage devices for next generation transport technologies. Further advanced study of those proposed structures are ongoing within our group

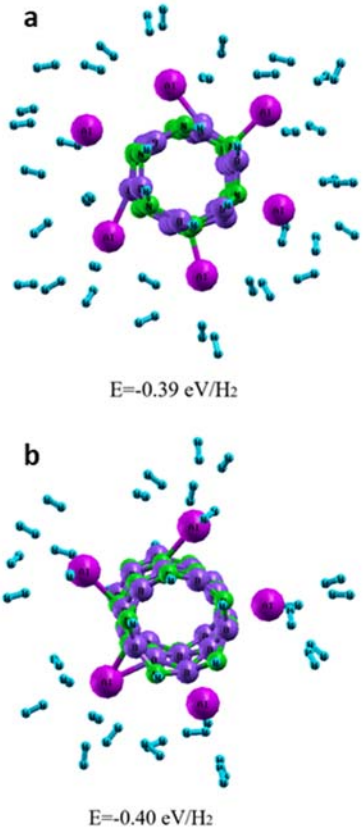

Figure 10. Top-down view of the energy minima of a) ***36*H$_2$⋂*6*Al@BNNT(3,3)** and b) ***30*H$_2$⋂*5*Al@BNNT(5,0)**

4. Conclusion:

The H_2 storage capacity of Al-decorated zigzag and armchair polymorphs of BNNTs was examined using first principle density functional theory that are suitable for accurately predicting

the structural and energetic of 2D materials. The first readily chemisorbed aluminum sits roughly over the centroid of the BN hexagon in both cases, but in the case of ***1*Al@BNNT(3,3)**, the metal interacts equally with two of the nitrogen atoms, while for ***1*Al@BNNT(5,0)**, the metal interacts preferentially with just one of the nitrogen atoms. This difference in symmetry leads to all the other differences between the two systems, significantly changing the dipole moment and charge density on the aluminum atom. The physisorption of a single H_2 onto either system induces minor changes to the electric field around the Al atom, which in turn subtly affects the charge distributions on nearby B and N atoms. This charge transfer enhances the magnitude of the dipole moment of ***1*H$_2$⋂*1*Al@BNNT** with respect to ***1*Al@BNNT**. For either polymorph, the single Al atom is able to adsorb up to six H_2 molecules. This binding event is within the desirable window for facile ambient temperature absorption and desorption required for an effective hydrogen storage device. In contrast, peralumination results in a far weaker Al-BNNT interaction and is not thermodynamically favorable (relative to the formation of Al-Al clusters). This could potentially be resolved by the formation of Al-nanoclusters on the surface of the BNNT and these studies are underway in the group to explore these more complicated systems. Should the synthetic challenge to access these materials be addressed, the two polymorphs prefer different numbers and arrangements of aluminum atoms, and similarly prefer different numbers of hydrogen molecules generating ***36*H$_2$⋂*6*Al@BNNT(3,3)** and ***30*H$_2$⋂*5*Al@BNNT(5,0)** as the stable forms. The former is highly symmetric, while the latter is highly asymmetric with each aluminum binding to the surface through a different interaction, but in both cases the binding energy per adsorbed hydrogen is in the favorable region at 0.39 eV/H_2 and 0.40 eV/H_2 which are promising values for effective H_2 loading. These ideal structures translate into 9.45 and 8.61 weight% hydrogen loading respectively which is well above the targets laid out by the DOE. This study indicates that aluminum-doped BNNTs with their exceptional surface area and very low weight, could form a useful theoretical material for high capacity loading of hydrogen. However, the experimental challenges in creating unpassivated aluminum and the importance of keeping the storage medium completely oxygen-free mean that these materials are more of interest for the design of less oxygen-reactive bare metal-functionalized BNNTs for hydrogen storage.

5. Acknowledgements

A. Rahdar would like to thank the University of Zabol for financial support (UOZ-GR-9618-40) for this work. JFT gratefully acknowledges financial support from the Natural Sciences and Engineering Research Council of Canada (grant # 2018-06338). and the Ontario Government for an Early Researcher Award (2019). The authors declare no competing financial interest. SMT, JJH, SIS and JFT would like to thank the Compute Canada for providing the facilities of the Shared Hierarchical Academic Research Computing Network (SHARCNET: www.sharcnet.ca) to support this project. The authors declare no competing financial interests.

6. Supporting Information

The material contains additional figures showing the charge density plots and the Mulliken charge analysis in the aluminum-functionalized BNNTs. All coordinates for the optimized structures are also included.

7. References

1. Peters, G. P.; Andrew, R. M.; Canadell, J. G.; Friedlingstein, P.; Jackson, R. B.; Korsbakken, J. I.; Le Quéré, C.; Peregon, A., Carbon dioxide emissions continue to grow amidst slowly emerging climate policies. *Nat. Clim. Change* **2019,** *Early View*. DOI: 10.1038/s41558-019-0659-6

2. Jackson, R. B.; Le Quéré, C.; Andrew, R. M.; Canadell, J. G.; Korsbakken, J. I.; Liu, Z.; Peters, G. P.; Zheng, B., Global energy growth is outpacing decarbonization. *Environ. Res. Lett.* **2018,** *13* (12), 120401. DOI: 10.1088/1748-9326/aaf303

3. Core Writing Team *Climate change 2014: Synthesis report. Contribution of working groups I, II and III to the Fifth Assessment Report of the Intergovernmental Panel on Climate Change*; IPCC: Geneva, Switzerland, 2014. URL:

4. Lewis, S. L.; Maslin, M. A., Defining the Anthropocene. *Nature* **2015,** *519* (7542), 171-180. DOI: 10.1038/nature14258

5. Eliasson, J.; Proost, S., Is sustainable transport policy sustainable? *Transp. Pol.* **2015,** *37*, 92-100. DOI: 10.1016/j.tranpol.2014.09.010

6. DOE Technical Targets for Onboard Hydrogen Storage for Light-Duty Vehicles. Department of Energy, Ed. United States Government: Washington DC, 2019.

7. (a) Dillon, A. C.; Jones, K. M.; Bekkedahl, T. A.; Kiang, C. H.; Bethune, D. S.; Heben, M. J., Storage of hydrogen in single-walled carbon nanotubes. *Nature* **1997,** *386* (6623), 377-379. DOI: 10.1038/386377a0 ; (b) Bhatia, S. K.; Myers, A. L., Optimum conditions for adsorptive storage. *Langmuir* **2006,** *22* (4), 1688-1700. DOI: 10.1021/la0523816

8. Ghosh, S.; Padmanabhan, V., Adsorption of hydrogen on single-walled carbon nanotubes with defects. *Diamond Relat. Mater.* **2015,** *59*, 47-53. DOI: 10.1016/j.diamond.2015.09.004

9. Sakintuna, B.; Lamaridarkrim, F.; Hirscher, M., Metal hydride materials for solid hydrogen storage: A review☆. *Int. J. Hydrogen Energy* **2007,** *32* (9), 1121-1140. DOI: 10.1016/j.ijhydene.2006.11.022

10. Amirante, R.; Cassone, E.; Distaso, E.; Tamburrano, P., Overview on recent developments in energy storage: Mechanical, electrochemical and hydrogen technologies. *Energy Convers. Manage.* **2017,** *132*, 372-387. DOI: 10.1016/j.enconman.2016.11.046

11. Schneemann, A.; White, J. L.; Kang, S.; Jeong, S.; Wan, L. F.; Cho, E. S.; Heo, T. W.; Prendergast, D.; Urban, J. J.; Wood, B. C.; Allendorf, M. D.; Stavila, V., Nanostructured metal hydrides for hydrogen storage. *Chem. Rev.* **2018,** *118* (22), 10775-10839. DOI: 10.1021/acs.chemrev.8b00313
12. (a) Liu, Y.; Brown, C. M.; Neumann, D. A.; Geohegan, D. B.; Puretzky, A. A.; Rouleau, C. M.; Hu, H.; Styers-Barnett, D.; Krasnov, P. O.; Yakobson, B. I., Metal-assisted hydrogen storage on Pt-decorated single-walled carbon nanohorns. *Carbon* **2012,** *50* (13), 4953-4964. DOI: 10.1016/j.carbon.2012.06.028 ; (b) Rather, S. u., Hydrogen uptake of manganese oxide-multiwalled carbon nanotube composites. *Int. J. Hydrogen Energy* **2019,** *44* (1), 325-331. DOI: 10.1016/j.ijhydene.2018.03.009 ; (c) Lueking, A.; Yang, R. T., Hydrogen storage in carbon nanotubes: Residual metal content and pretreatment temperature. *AIChE J.* **2003,** *49* (6), 1556-1568. DOI: 10.1002/aic.690490619
13. Rowsell, J. L. C.; Yaghi, O. M., Strategies for hydrogen storage in metal-organic frameworks. *Angew. Chem. Int. Ed.* **2005,** *44* (30), 4670-4679. DOI: 10.1002/anie.200462786
14. (a) Broom, D. P.; Webb, C. J., Pitfalls in the characterisation of the hydrogen sorption properties of materials. *Int. J. Hydrogen Energy* **2017,** *42* (49), 29320-29343. DOI: 10.1016/j.ijhydene.2017.10.028 ; (b) Yang, R. T., Hydrogen storage by alkali-doped carbon nanotubes–revisited. *Carbon* **2000,** *38* (4), 623-626. DOI: 10.1016/S0008-6223(99)00273-0
15. Chopra, N. G.; Luyken, R. J.; Cherrey, K.; Crespi, V. H.; Cohen, M. L.; Louie, S. G.; Zettl, A., Boron nitride nanotubes. *Science* **1995,** *269* (5226), 966-967. DOI: 10.1126/science.269.5226.966
16. (a) Golberg, D.; Bando, Y.; Tang, C. C.; Zhi, C. Y., Boron nitride nanotubes. *Adv. Mater. (Weinheim, Ger.)* **2007,** *19* (18), 2413-2432. DOI: 10.1002/adma.200700179 ; (b) Weng, Q.; Wang, X.; Wang, X.; Bando, Y.; Golberg, D., Functionalized hexagonal boron nitride nanomaterials: emerging properties and applications. *Chem. Soc. Rev.* **2016,** *45* (14), 3989-4012. DOI: 10.1039/C5CS00869G
17. (a) Bengu, E.; Marks, L. D., Single-walled BN nanostructures. *Phys. Rev. Lett.* **2001,** *86* (11), 2385-2387. DOI: 10.1103/physrevlett.86.2385 ; (b) Blase, X.; Rubio, A.; Louie, S. G.; Cohen, M. L., Stability and band gap constancy of boron nitride nanotubes. *Europhys. Lett.* **1994,** *28* (5), 335-340. DOI: 10.1209/0295-5075/28/5/007
18. (a) Froudakis, G. E., Hydrogen storage in nanotubes & nanostructures. *Mater. Today* **2011,** *14* (7-8), 324-328. DOI: 10.1016/s1369-7021(11)70162-6 ; (b) Mpourmpakis, G.; Froudakis, G. E., Why boron nitride nanotubes are preferable to carbon nanotubes for hydrogen storage? An *ab initio* theoretical study. *Catal. Today* **2007,** *120* (3-4), 341-345. DOI: 10.1016/j.cattod.2006.09.023
19. Zhou, Z.; Zhao, J.; Chen, Z.; Gao, X.; Yan, T.; Wen, B.; Schleyer, P. v. R., Comparative study of hydrogen adsorption on carbon and BN nanotubes. *J. Phys. Chem. B* **2006,** *110* (27), 13363-13369. DOI: 10.1021/jp0622740
20. (a) Ma, R.; Bando, Y.; Sato, T.; Golberg, D.; Zhu, H.; Xu, C.; Wu, D., Synthesis of boron nitride nanofibers and measurement of their hydrogen uptake capacity. *Appl. Phys. Lett.* **2002,** *81* (27), 5225-5227. DOI: 10.1063/1.1534415 ; (b) Ma, R.; Bando, Y.; Zhu, H.; Sato, T.; Xu, C.; Wu, D., Hydrogen uptake in boron nitride nanotubes at room temperature. *J. Am. Chem. Soc.* **2002,** *124* (26), 7672-7673. DOI: 10.1021/ja026030e
21. Tang, C.; Bando, Y.; Ding, X.; Qi, S.; Golberg, D., Catalyzed collapse and enhanced hydrogen storage of BN nanotubes. *J. Am. Chem. Soc.* **2002,** *124* (49), 14550-14551. DOI: 10.1021/ja028051e
22. Lei, W.; Zhang, H.; Wu, Y.; Zhang, B.; Liu, D.; Qin, S.; Liu, Z.; Liu, L.; Ma, Y.; Chen, Y., Oxygen-doped boron nitride nanosheets with excellent performance in hydrogen storage. *Nano Energy* **2014,** *6*, 219-224. DOI: 10.1016/j.nanoen.2014.04.004
23. Zhang, L. P.; Wu, P.; Sullivan, M. B., Hydrogen adsorption on Rh, Ni, and Pd functionalized single-walled boron nitride nanotubes. *J. Phys. Chem. C* **2011,** *115* (10), 4289-4296. DOI: 10.1021/jp1078554
24. (a) Yildirim, T.; Ciraci, S., Titanium-decorated carbon nanotubes as a potential high-capacity hydrogen storage medium. *Phys. Rev. Lett.* **2005,** *94* (17). DOI: 10.1103/physrevlett.94.175501 ; (b) Mananghaya, M. R., Hydrogen saturation limit of Ti-doped BN nanotube with B-N defects: An insight from DFT calculations. *Int. J. Hydrogen Energy* **2018,** *43* (22), 10368-10375. DOI: 10.1016/j.ijhydene.2018.04.037 ; (c) Durgun, E.; Jang, Y. R.; Ciraci, S., Hydrogen storage capacity of Ti-doped boron-nitride and B/Be-substituted carbon nanotubes. *Phys. Rev. B* **2007,** *76* (7), 073413. DOI:

10.1103/PhysRevB.76.073413 ; (d) Mananghaya, M. R., Titanium-decorated boron nitride nanotubes for hydrogen storage: a multiscale theoretical investigation. *Nanoscale* **2019,** *11* (34), 16052-16062. DOI: 10.1039/C9NR04578C
25. (a) Shayeganfar, F.; Shahsavari, R., Oxygen- and lithium-doped hybrid boron-nitride/carbon networks for hydrogen storage. *Langmuir* **2016,** *32* (50), 13313-13321. DOI: 10.1021/acs.langmuir.6b02997 ; (b) Bhattacharya, S.; Majumder, C.; Das, G. P., Hydrogen storage in Ti-decorated BC_4N nanotube. *J. Phys. Chem. C* **2008,** *112* (45), 17487-17491. DOI: 10.1021/jp807280w ; (c) Jhi, S.-H.; Kwon, Y.-K., Hydrogen adsorption on boron nitride nanotubes: A path to room-temperature hydrogen storage. *Phys. Rev. B* **2004,** *69* (24), 245407. DOI: 10.1103/PhysRevB.69.245407
26. (a) Li, X. M.; Tian, W. Q.; Huang, X.-R.; Sun, C.-C.; Jiang, L., Adsorption of hydrogen on novel Pt-doped BN nanotube: A density functional theory study. *J. Mol. Struct.: THEOCHEM* **2009,** *901* (1), 103-109. DOI: 10.1016/j.theochem.2009.01.019 ; (b) Wu, X.; Yang, J. L.; Zeng, X. C., Adsorption of hydrogen molecules on the platinum-doped boron nitride nanotubes. *J. Chem. Phys.* **2006,** *125* (4), 044704. DOI: 10.1063/1.2210933
27. Zhang, Z.-W.; Zheng, W.-T.; Jiang, Q., Hydrogen adsorption on Ce/BNNT systems: A DFT study. *Int. J. Hydrogen Energy* **2012,** *37* (6), 5090-5099. DOI: 10.1016/j.ijhydene.2011.12.036
28. Qiu, N.-x.; Tian, Z.-y.; Guo, Y.; Zhang, C.-h.; Luo, Y.-p.; Xue, Y., A first-principle study of calcium-decorated BC2N sheet doped by boron or carbon for high hydrogen storage. *Int. J. Hydrogen Energy* **2014,** *39* (17), 9307-9320. DOI: 10.1016/j.ijhydene.2014.04.063
29. Tang, C.; Zhang, X.; Zhou, X., Most effective way to improve the hydrogen storage abilities of Na-decorated BN sheets: applying external biaxial strain and an electric field. *Phys. Chem. Chem. Phys.* **2017,** *19* (7), 5570-5578. DOI: 10.1039/C6CP07433B
30. Qi, P.; Zhang, Y.; Chen, H., Li-coated B36N24 as potential hydrogen storage material. *Comput. Theor. Chem.* **2014,** *1047*, 30-37. DOI: 10.1016/j.comptc.2014.08.013
31. Khan, M. S.; Khan, M. S., Computational study of hydrogen adsorption on potassium-decorated boron nitride nanotubes. *Int. Nano Lett.* **2011,** *1* (2), 103-110. DOI: None Assigned
32. Cui, X.-Y.; Jia, J.-F.; Yang, B.-S.; Yang, P.; Wu, H.-S., *Ab initio* investigation of hydrogenation of endohedral X@(BN)16 complexes (X=Li^+, Na^+, K^+, Mg^{2+}, Ne, O^{2-}, S^{2-}, F^-, Cl^-). *J. Mol. Struct.: THEOCHEM* **2010,** *953* (1), 1-6. DOI: 10.1016/j.theochem.2010.03.016
33. Lale, A.; Bernard, S.; Demirci, U. B., Boron nitride for hydrogen storage. *ChemPlusChem* **2018,** *83* (10), 893-903. DOI: 10.1002/cplu.201800168
34. Seenithurai, S.; Pandyan, R. K.; Kumar, S. V.; Saranya, C.; Mahendran, M., Al-decorated carbon nanotube as the molecular hydrogen storage medium. *Int. J. Hydrogen Energy* **2014,** *39* (23), 11990-11998. DOI: 10.1016/j.ijhydene.2014.05.184
35. (a) Ao, Z. M.; Peeters, F. M., High-capacity hydrogen storage in Al-adsorbed graphene. *Phys. Rev. B* **2010,** *81* (20), 205406. DOI: 10.1103/PhysRevB.81.205406 ; (b) Ao, Z.; Dou, S.; Xu, Z.; Jiang, Q.; Wang, G., Hydrogen storage in porous graphene with Al decoration. *International Journal of Hydrogen Energy* **2014,** *39* (28), 16244-16251. DOI: https://doi.org/10.1016/j.ijhydene.2014.01.044 ; (c) Ao, Z. M.; Jiang, Q.; Zhang, R. Q.; Tan, T. T.; Li, S., Al doped graphene: A promising material for hydrogen storage at room temperature. *Journal of Applied Physics* **2009,** *105* (7), 074307. DOI: 10.1063/1.3103327 ; (d) Ao, Z. M.; Yang, J.; Li, S.; Jiang, Q., Enhancement of CO detection in Al doped graphene. *Chemical Physics Letters* **2008,** *461* (4), 276-279. DOI: https://doi.org/10.1016/j.cplett.2008.07.039
36. Pukazhselvan, D.; Gupta, B. K.; Srivastava, A.; Srivastava, O. N., Investigations on hydrogen storage behavior of CNT doped $NaAlH_4$. *J. Alloys Compd.* **2005,** *403* (1), 312-317. DOI: 10.1016/j.jallcom.2005.05.008
37. (a) Kawakami, Y.; Nojima, Y.; Doi, K.; Nakamura, K.; Tachibana, A., First-principle study on structures and electronic properties of aluminum nanowire wrapped in carbon nanotube. *Electrochim. Acta* **2004,** *50* (2), 739-744. DOI: 10.1016/j.electacta.2003.12.082 ; (b) Nakano, H.; Ohta, H.; Yokoe, A.; Doi, K.; Tachibana, A., First-principle molecular-dynamics study of hydrogen adsorption on an aluminum-doped carbon nanotube. *J. Power Sources* **2006,** *163* (1), 125-134. DOI: 10.1016/j.jpowsour.2006.04.023

38. Muniyandi, S.; Sundaram, R.; Kar, T., Aluminum doping makes boron nitride nanotubes (BNNTs) an attractive adsorbent of hydrazine (N_2H_4). *Struct. Chem.* **2018,** *29* (1), 375-382. DOI: 10.1007/s11224-017-1034-8
39. Ahmadi Peyghan, A.; Hadipour, N. L.; Bagheri, Z., Effects of Al doping and double-antisite defect on the adsorption of HCN on a BC_2N nanotube: Density functional theory studies. *J. Phys. Chem. C* **2013,** *117* (5), 2427-2432. DOI: 10.1021/jp312503h
40. Heidari, H.; Afshari, S.; Habibi, E., Sensing properties of pristine, Al-doped, and defected boron nitride nanosheet toward mercaptans: A first-principles study. *RSC Adv.* **2015,** *5* (114), 94201-94209. DOI: 10.1039/C5RA09923D
41. Lu, N.; Wei, W.; Chuai, X.; Mei, Y.; Li, L.; Liu, M. In *Investigation of adsorbed small-molecule on boron nitride nanotube (BNNT) based on first-principles calculations*, 2018 International Conference on Simulation of Semiconductor Processes and Devices (SISPAD), 24-26 Sept. 2018; 2018; pp 284-287.
42. Zhang, S.; Wu, B.; Wu, X. K.; Jing, T., The structural and hydrogen storage properties of Al-doped boron nitride nanotube. *Appl. Mech. Mater.* **2014,** *672-674*, 712-715. DOI: 10.4028/www.scientific.net/AMM.672-674.712
43. Lee, R. S.; Gavillet, J.; Chapelle, M. L. d. l.; Loiseau, A.; Cochon, J. L.; Pigache, D.; Thibault, J.; Willaime, F., Catalyst-free synthesis of boron nitride single-wall nanotubes with a preferred zig-zag configuration. *Phys. Rev. B* **2001,** *64* (12), 121405. DOI: 10.1103/PhysRevB.64.121405
44. Loiseau, A.; Willaime, F.; Demoncy, N.; Schramchenko, N.; Hug, G.; Colliex, C.; Pascard, H., Boron nitride nanotubes. *Carbon* **1998,** *36* (5), 743-752. DOI: 10.1016/S0008-6223(98)00040-2
45. (a) Giannozzi, P.; Andreussi, O.; Brumme, T.; Bunau, O.; Buongiorno Nardelli, M.; Calandra, M.; Car, R.; Cavazzoni, C.; Ceresoli, D.; Cococcioni, M.; Colonna, N.; Carnimeo, I.; Dal Corso, A.; De Gironcoli, S.; Delugas, P.; Distasio, R. A.; Ferretti, A.; Floris, A.; Fratesi, G.; Fugallo, G.; Gebauer, R.; Gerstmann, U.; Giustino, F.; Gorni, T.; Jia, J.; Kawamura, M.; Ko, H. Y.; Kokalj, A.; Küçükbenli, E.; Lazzeri, M.; Marsili, M.; Marzari, N.; Mauri, F.; Nguyen, N. L.; Nguyen, H. V.; Otero-De-La-Roza, A.; Paulatto, L.; Poncé, S.; Rocca, D.; Sabatini, R.; Santra, B.; Schlipf, M.; Seitsonen, A. P.; Smogunov, A.; Timrov, I.; Thonhauser, T.; Umari, P.; Vast, N.; Wu, X.; Baroni, S., Advanced capabilities for materials modelling with Quantum ESPRESSO. *J. Phys.: Condens. Matter* **2017,** *29* (46), 465901. DOI: 10.1088/1361-648x/aa8f79 ; (b) Giannozzi, P.; Baroni, S.; Bonini, N.; Calandra, M.; Car, R.; Cavazzoni, C.; Ceresoli, D.; Chiarotti, G. L.; Cococcioni, M.; Dabo, I.; Dal Corso, A.; De Gironcoli, S.; Fabris, S.; Fratesi, G.; Gebauer, R.; Gerstmann, U.; Gougoussis, C.; Kokalj, A.; Lazzeri, M.; Martin-Samos, L.; Marzari, N.; Mauri, F.; Mazzarello, R.; Paolini, S.; Pasquarello, A.; Paulatto, L.; Sbraccia, C.; Scandolo, S.; Sclauzero, G.; Seitsonen, A. P.; Smogunov, A.; Umari, P.; Wentzcovitch, R. M., QUANTUM ESPRESSO: a modular and open-source software project for quantum simulations of materials. *J. Phys.: Condens. Matter* **2009,** *21* (39), 395502. DOI: 10.1088/0953-8984/21/39/395502
46. Kohn, W.; Sham, L. J., Self-consistent equations including exchange and correlation effects. *Phys. Rev.* **1965,** *140* (4A), A1133-A1138. DOI: 10.1103/physrev.140.a1133
47. Takeda, T., The scalar relativistic approximation. *Z. Phys. B Conden. Matter* **1978,** *32* (1), 43-48. DOI: 10.1007/bf01322185
48. Hestenes, M. R.; Stiefel, E., Methods of conjugate gradients for solving linear systems. *J. Res. Nat. Bur. Stand.* **1952,** *49* (6), 409-436. DOI: None Assigned
49. Kokalj, A. *PWgui*, 6.1; Jozef Stefan Institute: Ljubljana, Slovenia, 2017.
50. Kokalj, A. *XCrySDen*, 1.6; Jozef Stefan Institute: Ljubljana, Slovenia, 2019.
51. Frisch, M. J.; Trucks, G. W.; Schlegel, H. B.; Scuseria, G. E.; Robb, M. A.; Cheeseman, J. R.; Scalmani, G.; Barone, V.; Mennucci, B.; Petersson, G. A.; Nakatsuji, H.; Caricato, M.; Li, X.; Hratchian, H. P.; Izmaylov, A. F.; Bloino, J.; Zheng, G.; Sonnenberg, J. L.; Hada, M.; Ehara, M.; Toyota, K.; Fukuda, R.; Hasegawa, J.; Ishida, M.; Nakajima, T.; Honda, Y.; Kitao, O.; Nakai, H.; Vreven, T.; Montgomery Jr., J. A.; Peralta, J. E.; Ogliaro, F.; Bearpark, M. J.; Heyd, J.; Brothers, E. N.; Kudin, K. N.; Staroverov, V. N.; Kobayashi, R.; Normand, J.; Raghavachari, K.; Rendell, A. P.; Burant, J. C.; Iyengar, S. S.; Tomasi, J.; Cossi, M.; Rega, N.; Millam, N. J.; Klene, M.; Knox, J. E.; Cross, J. B.; Bakken, V.; Adamo, C.; Jaramillo, J.; Gomperts, R.; Stratmann, R. E.; Yazyev, O.; Austin, A. J.; Cammi, R.; Pomelli, C.; Ochterski, J. W.;

Martin, R. L.; Morokuma, K.; Zakrzewski, V. G.; Voth, G. A.; Salvador, P.; Dannenberg, J. J.; Dapprich, S.; Daniels, A. D.; Farkas, Ö.; Foresman, J. B.; Ortiz, J. V.; Cioslowski, J.; Fox, D. J. *Gaussian 09*, Gaussian, Inc.: Wallingford, CT, USA, 2009.
52. (a) Golberg, D.; Bando, Y., Unique morphologies of boron nitride nanotubes. *Appl. Phys. Lett.* **2001,** *79* (3), 415-417. DOI: 10.1063/1.1385188 ; (b) Ma, R.; Bando, Y.; Sato, T.; Kurashima, K., Growth, morphology, and structure of boron nitride nanotubes. *Chem. Mater.* **2001,** *13* (9), 2965-2971. DOI: 10.1021/cm0102741
53. Chandrakumar, K. R. S.; Srinivasu, K.; Ghosh, S. K., Nanoscale curvature-induced hydrogen adsorption in alkali metal doped carbon nanomaterials. *J. Phys. Chem. C* **2008,** *112* (40), 15670-15679. DOI: 10.1021/jp8019446
54. Zeynali, S.; Ketabi, S.; Aghabozorg, H. R., Density functional study of hydrogen adsorption on alkali metal doped carbon nanotube. *J. Comput. Theor. Nanosci.* **2014,** *11* (5), 1317-1322. DOI: 10.1166/jctn.2014.3498
55. (a) Rosi, N. L.; Eckert, J.; Eddaoudi, M.; Vodak, D. T.; Kim, J.; O'Keefe, M.; Yaghi, O. M., Hydrogen storage in microporous metal-organic frameworks. *Science* **2003,** *300* (5622), 1127-1129. DOI: 10.1126/science.1083440 ; (b) Abdalla, A. M.; Hossain, S.; Nisfindy, O. B.; Azad, A. T.; Dawood, M.; Azad, A. K., Hydrogen production, storage, transportation and key challenges with applications: A review. *Energy Convers. Manage.* **2018,** *165*, 602-627. DOI: 10.1016/j.enconman.2018.03.088
56. Gaudoin, R.; Foulkes, W. M. C.; Rajagopal, G., *Ab initio* calculations of the cohesive energy and the bulk modulus of aluminium. *J. Phys.: Condens. Matter* **2002,** *14* (38), 8787-8793. DOI: 10.1088/0953-8984/14/38/303

Table of Contents Graphic